

Vector-Quantized Vision Foundation Models for Object-Centric Learning

Rongzhen Zhao Vivienne Wang Juho Kannala Joni Pajarinen

Aalto University, Espoo, Finland

{rongzhen.zhao, vivienne.wang, juho.kannala, joni.pajarinen}@aalto.fi

Abstract

Decomposing visual scenes into objects, as humans do, facilitates modeling object relations and dynamics. Object-Centric Learning (OCL) achieves this by aggregating image or video feature maps into object-level feature vectors, known as *slots*. OCL’s self-supervision via reconstructing the input from slots struggles with complex textures, thus many methods employ Vision Foundation Models (VFMs) to extract feature maps with better objectness. However, using VFMs merely as feature extractors does not fully unlock their potential. We propose Vector-Quantized VFMs for OCL (VQ-VFM-OCL, or VVO), where VFM features are extracted to facilitate object-level information aggregation and further quantized to strengthen supervision in reconstruction. Our VVO unifies OCL representatives into a concise architecture. Experiments demonstrate that VVO not only outperforms mainstream methods on object discovery tasks but also benefits downstream tasks like visual prediction and reasoning. The source code is available in the supplement.

1. Introduction

Objects can form highly diverse visual scenes through arrangements and combinations. But mainstream methods based on feature patches or a single feature vector disregard such compositionality. Inspired by human vision cognition (Bar, 2004; Cavanagh, 2011; Palmeri & Gauthier, 2004), Object-Centric Learning (OCL) decomposes visual scenes into multiple feature vectors, known as *slots*, each corresponding to an object or the background, thus enabling improved modeling of relationships and dynamics among objects. Object-centric representations have demonstrated superiority in advanced vision tasks, like prediction, reasoning, planning, and decision-making (Wu et al., 2023a).

Existing OCL methods typically adopt an encoder-aggregator-decoder architecture (Locatello et al., 2020). Firstly, the encoder transforms input image or video frame

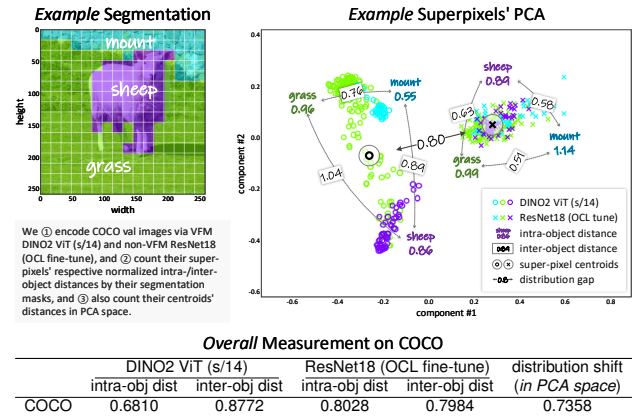


Figure 1. We utilize two observations: (i) Compared to non-VFMs, VFMs extract features with better object separability, i.e., smaller intra-object distances and larger inter-object distances \Rightarrow We facilitate OCL aggregation via VFM features; (ii) VFM and non-VFM features have a distribution gap, i.e., far-flung centroids \Rightarrow We strengthen OCL supervision by sharing the aforementioned VFM features and quantizing them as the reconstruction target.

pixels into a dense feature map. Then, the aggregator sparsifies this feature map into feature vectors via Slot Attention (Locatello et al., 2020) with initial slots. Lastly, the decoder reconstructs the input in some form from these slots, to provide the self-supervised training signal.

Due to its self-supervision nature, OCL heavily relies on pixel textures to separate different objects. The early milestone (Locatello et al., 2020) reconstructs input pixels for supervision, which usually fails on realistic objects with complex textures. Some methods (Kipf et al., 2022; Elsayed et al., 2022) reconstruct the optical flow or depth map of the input to mitigate textural noises, albeit at the cost of extra expensive annotations. Some others (Singh et al., 2022a;c) reconstruct input’s VAE (Variational Autoencoder) representation, where super-pixels are codebook codes shared across samples, thus suppressing pixel redundancy and facilitating aggregation from the feature map into slots. Recent advances (Seitzer et al., 2023; Wu et al., 2023b) leverage Vision Foundation Models (VFMs) (Caron et al., 2021; Oquab et al., 2023) to extract feature maps with better object sepa-

rability, significantly improving OCL performance.

However, these methods merely treat VFMs as stronger feature extractors for OCL encoding, overlooking their potential to provide better reconstruction targets for OCL decoding. VFMs have yet to be fully utilized in OCL.

We propose *Vector-Quantized Vision Foundation Models for Object-Centric Learning*, VQ-VFM-OCL or VVO. As shown in Figure 1, we fully utilize VFMs in OCL in two ways. We not only use VFMs to extract feature maps with better objectness, to facilitate object information aggregation. We also quantize VFM feature maps with codebook codes, to strengthen supervision in reconstruction. Such shared quantization suppresses redundant feature information and produces consistent reconstruction targets across samples, facilitating aggregation via those initial slots, which are also shared across samples.

Our contributions are: (i) A unified architecture of encoder-aggregator/quantizer-decoder, which supports various OCL modules; (ii) Three key designs of direct VFM feature extraction, shared VFM feature quantization to fully utilize VFMs in OCL, and a VQ variant designed for OCL; (iii) Significant improvements in mainstream OCL methods, along with benefits to downstream task performance.

2. Related Work

SSseg vs OCL. Both Self-Supervised Segmentation (SSseg) (Ge et al., 2023; Wang et al., 2024) and OCL can discover objects, i.e., segment object, in images or videos without supervision. But SSseg only outputs object segmentation masks, while OCL represents objects as *slots* with segmentation as byproduct. Besides, these slots can be directly used in downstream object-centric world models (Wu et al., 2023a) for dynamics modeling, which is demanded in advanced vision tasks, like prediction, reasoning, planning and decision-making. A direct comparison between OCL and SSseg methods is beyond the scope of this work.

OCL encoding. The stronger encoder that extracts feature maps of better objectness contributes more to OCL performance. Early milestone methods like IODINE (Greff et al., 2019) and SA (Locatello et al., 2020) use small naive CNNs (Krizhevsky et al., 2012) as OCL encoder. Followups like SAVi (Kipf et al., 2022), SAVi++ (Elsayed et al., 2022), SLATE (Singh et al., 2022a) and STEVE (Singh et al., 2022c) employ pretrained ResNets (He et al., 2016), and fine-tune them in OCL. State-of-the-arts like SlotDiffusion (Wu et al., 2023b) and DINOSAUR (Seitzer et al., 2023) utilize VFMs DINO (Caron et al., 2021) and DINO2 (Oquab et al., 2023) ViTs (Vision Transformers) to extract highly object-separable feature map from input pixels, improving OCL performance significantly. Although SAM (Kirillov et al., 2023) and SAM2 (Ravi et al., 2024) are also recog-

nized VFMs, they remain unexploited in OCL setting. Our VVO supports various VFMs for OCL encoding.

OCL aggregation. SlotAttention (Locatello et al., 2020) is the footstone for mainstream OCL methods. Subsequent works like BO-QSA (Jia et al., 2023), ISA (Biza et al., 2023) and SysBind (Singh et al., 2022b) are all its variants, which are all designed without changing the external interface. But considering their performance boosts, where some are very limited, we only integrate BO-QSA by default.

OCL decoding. With SlotAttention as the aggregator, the decoder and its reconstruction target affect OCL performance the most, as it is the source of supervision. Mixture-based decoding, used in SAVi, SAVi++, DINOSAUR and VideoSAUR (Zadaianchuk et al., 2024), decodes each slot’s spatial broadcast (Watters et al., 2019) using naive CNNs or MLPs, and mixes them with corresponding weights into the reconstruction. Transformer-based decoding, used in SLATE, STEVE and SPOT (Kakogeorgiou et al., 2024), reconstructs VAE representation of the input auto-regressively with slots as the condition. Diffusion-based decoding, used in LSD (Jiang et al., 2023) and SlotDiffusion, drives slots to recover noise added to the input’s VAE representation. Our VVO supports all these types of OCL decoding.

VAE for OCL. Variational Autoencoders (VAEs), like dVAE (Im Im et al., 2017) in SLATE and VQ-VAE (Van Den Oord et al., 2017) in SlotDiffusion, are employed to produce reconstruction targets for OCL training. Since these VAEs are designed for image generation, some methods adapt them for OCL. Inspired by channel or weight grouping, GDR (Zhao et al., 2024a) decomposes features into attributes and combine them to produce VAE representation as reconstruction targets to guide OCL better. MSF (Zhao et al., 2024b) exploits the multi-scale idea from detection and segmentation in OCL with novel VAE designs. Based on recent advancement RVQ (Yang et al., 2023) and SimVQ (Zhu et al., 2024), we design our own VQ variant for OCL.

3. Proposed Method

We propose Vector-Quantized Vision Foundation Models for Object-Centric Learning, or VQ-VFM-OCL (VVO), unifying mainstream OCL with significant performance boosts. Using VFMs for better performance is not new, but VVO is the first to fully utilize VFMs in the OCL setting.

3.1. Unify OCL

As shown in Figure 2, our method adopts an architectural design of encoder-aggregator/quantizer-decoder.

Firstly, OCL encoder ϕ_e transforms an input image or video frame $\mathbf{X} \in \mathbb{R}^{h_0 \times w_0 \times c_0}$, which is an observation of some visual scene, into a dense feature map $\mathbf{Z} \in \mathbb{R}^{h \times w \times c}$, for the

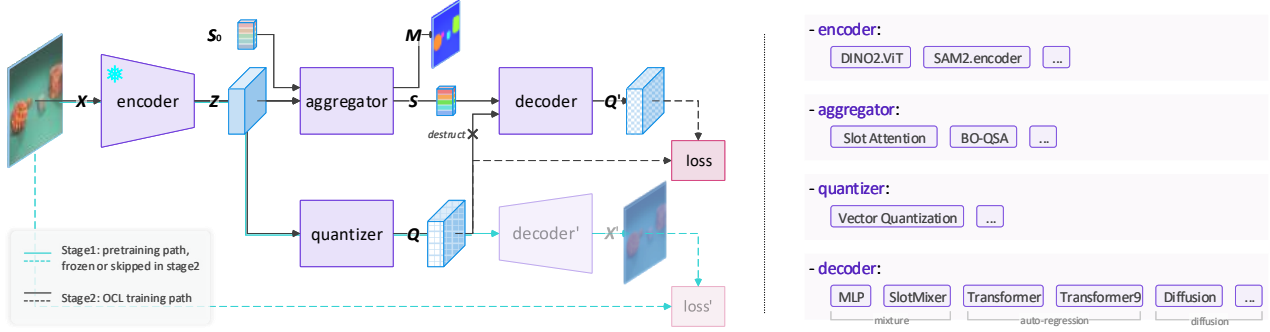


Figure 2. VVO is a unified architecture that fully utilizes VFMs in OCL. It not only extracts VFM features with better objectness to facilitate object information aggregation; but further quantizes those VFM features as reconstruction targets to strengthen OCL training supervision. With typical SlotAttention or its variants as the **aggregator** and Vector-Quantization as the **quantizer**, VVO supports different VFMs as the **encoder**, and supports mainstream mixture, auto-regression and diffusion models as the **decoder**.

following query-based aggregation:

$$\phi_e : \mathbf{X} \rightarrow \mathbf{Z} \quad (1)$$

where ϕ_e can be parameterized as pretrained frozen VFMs, like DINO (Caron et al., 2021), DINO2 (Oquab et al., 2023), SAM (Kirillov et al., 2023) and SAM2 (Ravi et al., 2024). As OCL relies on textures to separate objects, ϕ_e should handle complex textures of objects, making VFMs necessary here. We will detail the reasons in Section 3.2.

Secondly, given **queries** $\mathbf{S}_0 \in \mathbb{R}^{n \times c}$, OCL **aggregator** ϕ_a transforms \mathbf{Z} into multiple feature vectors or **slots** $\mathbf{S} \in \mathbb{R}^{n \times c}$ and byproduct **segmentation** masks $\mathbf{M} \in \mathbb{R}^{h \times w}$, corresponding to objects or the background in the scene:

$$\phi_a : (\mathbf{S}_0, \mathbf{Z}) \rightarrow (\mathbf{S}, \mathbf{M}) \quad (2)$$

where ϕ_a can be parameterized as widely adopted SlotAttention (Locatello et al., 2020) and its variants, which is some cross attention with \mathbf{S}_0 as queries and \mathbf{Z} as keys and values. \mathbf{M} is the binarized attention map thus intuitively reflects how well objects are represented by slots.

For video OCL, there is a recurrent module turning current \mathbf{S} into new queries \mathbf{S}_0 for the next time step. Such module can be Transformer encoder blocks (Vaswani et al., 2017).

Meanwhile, OCL **quantizer** ϕ_q transforms \mathbf{X} into the reconstruction **target** $\mathbf{Q} \in \mathbb{R}^{h \times w \times c}$ for the following decoding:

$$\phi_q : \mathbf{X} \rightarrow \mathbf{Q} \quad (3)$$

where ϕ_q can be parameterized as some Vector Quantization (VQ) module (Im Im et al., 2017; Van Den Oord et al., 2017). But we meticulously design our own VQ variant, as detailed in Section 3.2. ϕ_q is pretrained in VAE framework and is frozen afterwards, where the encoder is shared from the frozen OCL encoder ϕ_e , and the decoder is a typical VAE decoder. We will explain why not use a separate typical VAE encoder in Section 3.2.

Thirdly, OCL **decoder** ϕ_d transforms \mathbf{S} into **reconstruction** $\mathbf{Q}' \in \mathbb{R}^{h \times w \times c}$ with destructed \mathbf{Q} as the condition:

$$\phi_d : (\mathbf{S}, \mathbf{Q}) \rightarrow \mathbf{Q}' \quad (4)$$

where ϕ_d can be parameterized as a CNN or MLP if using mixture decoding for OCL (Kipf et al., 2022; Seitzer et al., 2023), where each of \mathbf{S} is spatially broadcast (Watters et al., 2019) into the shape of \mathbf{Q} and then decoded into a component and finally mixed together with predicted weights; or (ii) a Transformer decoder if using auto-regressive decoding (Singh et al., 2022a; Kakogeorgiou et al., 2024), where causally masked \mathbf{Q} is the query and \mathbf{S} is the key and value; or (iii) a conditional Diffusion model if using diffusion decoding (Wu et al., 2023b; Jiang et al., 2023), where \mathbf{Q} with noise is the input and \mathbf{S} is the condition.

Reconstructing the destructed \mathbf{Q} using \mathbf{S} drives \mathbf{S} to aggregate as much object information as possible. Thus, a good reconstruction target, like in (Zhao et al., 2024a;b), is very important. We will explain this in Section 3.2.

Lastly, the supervision signal for OCL training comes from minimizing the reconstruction **loss** between \mathbf{Q}' and \mathbf{Q} :

$$\min_{(\phi_a, \phi_d)} f_{\text{recon}}(\mathbf{Q}', \mathbf{Q}) \quad (5)$$

where $f_{\text{recon}}(\cdot, \cdot)$ can be (i) Mean Squared Error (MSE) loss for mixture and diffusion OCL decoding, or (ii) Cross Entropy (CE) loss for auto-regressive decoding.

3.2. Fully Utilize VFMs in OCL

We fully utilize VFMs in the OCL setting by two key designs: (i) direct VFM feature extraction to facilitate object-level information aggregation, and (ii) shared VFM feature quantization as reconstruction targets to strengthen supervision in OCL training.

Direct VFM Feature Extraction for Better Aggregation

We directly extract the feature map Z from the input X using VFMs as ϕ_e , where DINO2 ViT and SAM2 encoder are chosen and experimented thoroughly. No extra position encoding is needed here like in SA (Locatello et al., 2020) because these VFMs already contain the positional information required in ϕ_a . Since ϕ_e is frozen, We further use a trainable linear layer to adjust Z slightly. Thus, We expect the subsequent ϕ_a to aggregate dense Z into sparse slots S under queries S_0 better.

Direct use of VFMs for feature extraction contributes to better aggregation. As shown in Figure 1, VFM representations show better objectness or object separability than that of non-VFMs, under naive kMeans clustering¹. OCL aggregation based on SlotAttention and its variants is essentially a clustering whose initial centroids are trainable (Jia et al., 2023). This has already been empirically exploited in previous methods like DINOSAUR (Seitzer et al., 2023) and SlotDiffusion (Wu et al., 2023b), but without any explanation. We provide math analysis below.

Math Analysis: VFM Representation Eases Aggregation

As shown in Figure 3, super-pixels in a feature map Z all belong to two objects o_1 and o_2 , so two queries are needed for aggregation, which is basically sum of super-pixels weighted by normalized minus distances between queries and super-pixels (Locatello et al., 2020).

Denote the ideal query of o_2 as s_* , which is the clustering center or centroid of o_2 and is closer to all super-pixels in o_2 than in o_1 :

$$d_{*1} = d(s_*, v_1) > d(s_*, v_2) = d_{*2} \quad (6)$$

where $d(\cdot, \cdot)$ is a distance metric, e.g., minus inner product; v_1 and v_2 are arbitrary points in o_1 and o_2 , respectively.

But the actual query s follows $\mathcal{N}(s_*, \sigma^2 I)$. Substituting s

¹<https://scikit-learn.org/stable/modules/generated/sklearn.cluster.KMeans.html>

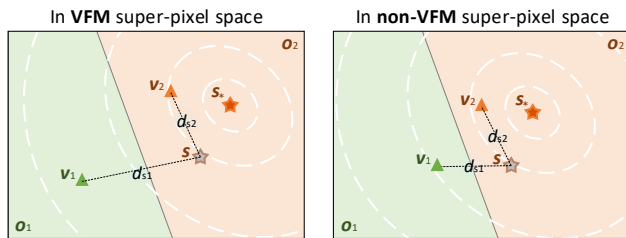


Figure 3. Better objectness helps OCL aggregation. Green and orange areas stand for objects o_1 and o_2 , where v_1 and v_2 are arbitrary super-pixels and s_* is o_2 's centroid. But the actual query $s \sim \mathcal{N}(s_*, \sigma^2)$. In VFM super-pixel space, the distance d_{12} between v_1 and v_2 is larger, i.e., better objectness, thus s has higher probability $p(d_{s1} > d_{s2})$ to represent o_2 correctly, compared with that in non-VFM super-pixel space.

for s_* , the probability of correct aggregation is:

$$p_2 = p(d_{s1} > d_{s2}) = \int_{v \in o_2} \frac{1}{\sqrt{2\pi}\sigma} e^{-\frac{1}{2}(\frac{v-s_*}{\sigma})^2} dv \quad (7)$$

where o_2 always contains s_* , and is bounded by the separation plane between o_1 and o_2 . The closer the boundary is to s_* the smaller p_2 is.

According to Figure 1, in VFM super-pixel space, points of the same object have smaller distances while points from different objects have larger distances, compared to that in non-VFM space. This means the separation plane is closer to s_* in non-VFM space. Therefore, p_2 in VFM space is bigger than in non-VFM space. \square

Shared VFM Feature Quantization for Better Supervision

Given the direct VFM feature map Z , we transform it with a naive CNN to eliminate the positional information for better quantization. We quantize the adjusted Z using our VQ variant as ϕ_q to obtain the reconstruction target Q .

Our VQ's codebook follows SimVQ (Zhu et al., 2024). We predefine $m = 4096$ template features, i.e., a codebook $T_0 \in \mathbb{R}^{m \times c_0}$, which are randomly initialized and remain frozen. In vector quantization, we project T with a pre-trainable linear layer and match it with the adjusted Z :

$$T := W \cdot \text{sg}(T_0) \quad (8)$$

$$D = \|Z - T\|_2^2 \quad (9)$$

where $\text{sg}(\cdot)$ is stop-gradient; $T \in \mathbb{R}^{m \times c}$ is the codebook to be used for quantizing Z ; $D \in \mathbb{R}^{h \times w \times m}$ is the matching distance between every super-pixel and every code.

We convert distances to probabilities and select the most matched codes to form the quantization Q :

$$P = \text{softmax}_c(-D) \quad (10)$$

$$I = \text{argmax}_m(P) \quad (11)$$

$$Q = \text{index}_m(T, I) \quad (12)$$

where $\text{softmax}(\cdot)$ is calculated along the channel dimension; P is the match probabilities; $I \in \mathbb{R}^{h \times w}$ is the matched code indexes; $\text{argmax}(\cdot)$ is calculated along the channel dimension; $\text{index}(\cdot, \cdot)$ is operated along code number dimension. The typical STE (Bengio et al., 2013) on Q , needed in pre-training, can be skipped during OCL training.

For its pre-training, we introduce some tricks. We add noise to D pre-Equation (10) to encourage code utilization:

$$D := \frac{D + G}{\tau} \quad (13)$$

where $G \in \mathbb{R}^{h \times w \times m}$ is the Gumbel noise and τ is the temperature. We devise annealing residual connection (Zhao et al., 2024a;b) post-Equation (12) to stabilize pre-training:

$$Q := \alpha Z + (1 - \alpha)Q \quad (14)$$

where α is scheduled from 1 to 0 during pre-training using cosine-annealing. Besides typical losses of reconstruction, alignment and commitment (Van Den Oord et al., 2017), we regularize the adjusted Z 's elements to be normalized:

$$l_n = \lambda \text{MSE}(Z, \text{sg}(\frac{Z - \mathbb{E}[Z]}{\sqrt{\mathbb{V}[Z]} + \epsilon})) \quad (15)$$

where λ is empirically set to 0.1; \mathbb{E} and \mathbb{V} are calculated along height, width and channel dimensions.

With all samples' feature maps Z being represented with one codebook T , the quantization Q naturally gains cross-sample consistency and suppresses information redundancy or noise. This helps the aggregation with queries S_0 , which are also shared across samples. After such tokenization, our reconstruction target can be either regressed using mixture and diffusion decoding or classified using auto-regressive decoding. In contrast, methods like SLATE (Singh et al., 2022a) and SlotDiffusion (Wu et al., 2023b) use separate VAE and OCL encoders, which as shown in Figure 1 causes a distribution gap between Q and Z . Thus, we expect shared VFM representation quantization as reconstruction targets to strengthen supervision.

Math Analysis: Shared VFM Representation Quantization Reduces Supervision Noise

We reconstruct Q' to approximate the target Q ultimately from Z via $\phi_a \circ \phi_d$, denoted as f for simplicity. Under MSE loss, the gradient with respect to Z is:

$$\frac{\partial \text{MSE}(Q', \text{sg}(Q))}{\partial Z} = 2(Q' - \text{sg}(Q)) \frac{\partial Q'}{\partial Z} \quad (16)$$

We obtain Q by quantizing Z , i.e., $\mathbb{E}[Z] = Q$, implying that any deviation of $Q' = f(Z)$ from Q is due to f and Z . Assuming f preserves Z 's statistical properties, we have:

$$\mathbb{E}[Q'] = \mathbb{E}[f(Z)] \approx Q \quad (17)$$

Thus the residual error $Q' - \text{sg}(Q)$ in Equation (16) is statistically unbiased and small on average:

$$\mathbb{E}[Q' - \text{sg}(Q)] \approx 0 \quad (18)$$

But if instead of sharing ϕ_e , we use an extra VAE encoder plus ϕ_a to obtain the target, denoted as Q_2 , then $Q_2 \neq Q$. Substitute Q_2 into Equation (16) and the residual error $Q' - \text{sg}(Q_2)$ would be systematically biased:

$$\mathbb{E}[Q' - \text{sg}(Q_2)] \neq 0 \quad (19)$$

which increases noise in optimization.

Using CE loss is slightly different but it does not alter our judgment above. \square

4. Experiment

We conduct all experiments using three random seeds.

4.1. Set up the Benchmark

Datasets. We include both synthetic and real-world datasets. ClevrTex² comprises synthetic images, each with about 10 geometric objects scattered in complex background. MOViD³ contains synthetic videos, each with up to 20 daily objects dropping and bumping. COCO⁴ is a recognized real-world image dataset, and we use its challenging panoptic segmentation. VOC⁵ is a real-world image dataset, and we use its instance segmentation. We also report results

²<https://www.robots.ox.ac.uk/~vgg/data/clevrtex>

³<https://github.com/google-research/kubric/blob/main/challenges/movi/README.md#movi-d>

⁴<https://cocodataset.org>

⁵<http://host.robots.ox.ac.uk/pascal/VOC>

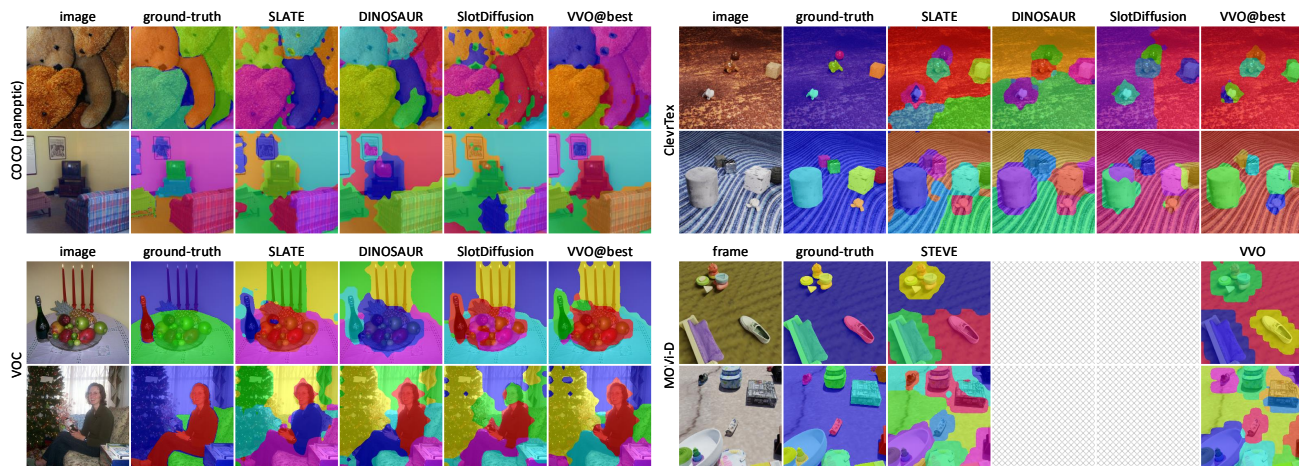


Figure 4. Qualitative object discovery performance comparison.

on real-world video dataset YTVIS⁶ version HQ⁷, which contains large-scale short videos from YouTube. We choose Physion⁸ for visual prediction and reasoning as it contains common object interactions, requiring algorithms to learn dynamics like support, roll and link, then to predict and reason about future scene states.

Models. We compare VVO with both OCL classics and state-of-the-arts. SLATE (Singh et al., 2022a) uses a Transformer decoder for auto-regressive decoding, and it differs from VVO in a separate VAE encoder and naive quantizer; STEVE (Singh et al., 2022c) is SLATE’s video version. DINOSAUR (Seitzer et al., 2023) uses an MLP for mixture decoding, and it differs from VVO in no quantization in its reconstruction target. SlotDiffusion (Wu et al., 2023b) uses a conditional Diffusion model for diffusion decoding, and it differs from VVO in a separate VAE encoder and naive quantizer. General improvers GDR (Zhao et al., 2024a) and MSF (Zhao et al., 2024b) only support auto-regression and diffusion decoding. We skip outdated methods like IODINE (Greff et al., 2019), SA (Locatello et al., 2020) and ISA (Biza et al., 2023) due to their low accuracy. We also skip SAVi (Kipf et al., 2022) and SAVi++ (Elsayed et al., 2022) as their extra modalities are unfair to others.

Comparison. Instead of copying existing results, we repro-

⁶<https://youtube-vos.org/dataset/vis>

⁷<https://github.com/SysCV/vmt?tab=readme-ov-file#hq-ytvis-high-quality-video-instance-segmentation-dataset>

⁸<https://physion-benchmark.github.io>

duce all baselines to realize fair comparison. As detailed in Appendices A and B, we use identical data augmentation, VFMs in OCL encoding and training recipes for all experiment items unless not applied. We instantiate all baselines’ VAE part as TAESD⁹, which is a large-scale pretrained StableDiffusion¹⁰ module, to build all *strong* baselines.

4.2. Evaluate on Object Discovery

Object discovery task intuitively shows how well those slots separate different objects. We evaluate the byproduct object segmentation accuracy with Adjusted Rand Index¹¹ (ARI), ARI_{fg} (foreground), mean Intersection-over-Union¹² (mIoU) and mean Best Overlap (Uijlings et al., 2013) (mBO).

With unsupervised pretrained VFMs for OCL encoding, i.e., DINO2 ViT (version s/14), our VVO is instantiated as VQDINO. As shown in Table 1, our method consistently improves object discovery performance across all types of OCL decoding. With a Transformer decoder Tfd for auto-regressive decoding, VVO significantly outperforms SLATE and STEVE across all datasets. With MLP MLP for mixture decoding, VVO shows a smaller advantage over DI-

⁹https://huggingface.co/docs/diffusers/en/api/models/autoencoder_tiny

¹⁰<https://huggingface.co/spaces/stabilityai/stable-diffusion>

¹¹https://scikit-learn.org/stable/modules/generated/sklearn.metrics.adjusted_rand_score.html

¹²https://scikit-learn.org/stable/modules/generated/sklearn.metrics.jaccard_score.html

resolution= 256×256	ClevrTex #slot=11				COCO (panoptic) #slot=7				VOC #slot=6				MOVi-D #slot=21, conditional			
	ARI	ARI _{fg}	mIoU	mBO	ARI	ARI _{fg}	mIoU	mBO	ARI	ARI _{fg}	mIoU	mBO	ARI	ARI _{fg}	mIoU	mBO
SLATE-DINO	15.8 _{±0.3}	85.8 _{±0.3}	26.2 _{±0.1}	40.0 _{±0.2}	34.4 _{±0.3}	35.4 _{±0.5}	7.1 _{±0.1}	26.8 _{±0.7}	16.4 _{±0.6}	22.2 _{±0.9}	13.0 _{±0.4}	34.7 _{±0.9}	—	—	—	—
VQDINO _{Tfd}	21.5 _{±0.2}	86.1 _{±0.1}	29.0 _{±0.1}	43.3 _{±0.1}	38.5 _{±0.4}	39.6 _{±0.4}	7.8 _{±0.0}	28.5 _{±0.4}	19.0 _{±0.9}	24.1 _{±0.7}	14.3 _{±0.3}	37.2 _{±0.8}	—	—	—	—
STEVE-DINO	—	—	—	—	—	—	—	—	—	—	—	—	35.0 _{±0.9}	64.1 _{±2.9}	21.2 _{±0.7}	23.2 _{±1.2}
VQDINO _{Tfdt}	—	—	—	—	—	—	—	—	—	—	—	—	41.4 _{±0.8}	70.5 _{±3.3}	23.1 _{±0.6}	25.9 _{±1.4}
DINOSAUR-DINO	18.5 _{±0.2}	87.8 _{±0.4}	26.7 _{±0.3}	39.9 _{±0.5}	35.3 _{±0.1}	36.4 _{±0.2}	7.1 _{±0.0}	27.3 _{±0.2}	18.8 _{±0.4}	31.2 _{±0.1}	14.4 _{±0.2}	37.9 _{±0.4}	—	—	—	—
VQDINO _{MLP}	51.2 _{±0.4}	88.3 _{±0.3}	29.8 _{±0.2}	44.6 _{±0.4}	35.4 _{±0.6}	36.7 _{±0.5}	7.6 _{±0.1}	27.7 _{±0.1}	20.6 _{±0.1}	32.9 _{±0.1}	15.6 _{±0.0}	39.1 _{±0.3}	—	—	—	—
SlotDiffusion-DINO	60.1 _{±0.4}	81.6 _{±2.7}	31.4 _{±0.9}	45.3 _{±0.9}	34.9 _{±0.4}	36.0 _{±0.4}	7.0 _{±0.2}	26.7 _{±0.6}	15.0 _{±0.3}	19.7 _{±0.4}	12.3 _{±0.2}	33.1 _{±0.3}	—	—	—	—
VQDINO _{Dfz}	37.9 _{±2.1}	81.7 _{±2.6}	29.3 _{±1.1}	47.8 _{±1.4}	37.2 _{±0.7}	38.3 _{±0.9}	7.3 _{±0.1}	27.8 _{±0.9}	17.8 _{±0.1}	24.1 _{±0.3}	14.1 _{±0.1}	36.1 _{±0.3}	—	—	—	—

Table 1. Object discovery performance with DINO2 ViT (s/14) for OCL encoding. VVO is instantiated as VQDINO; Tfd, Tfdt, MLP and Dfz are Transformer, Transformer-temporal, MLP and Diffusion for OCL decoding respectively.

resolution= 256×256	ClevrTex #slot=11				COCO (panoptic) #slot=7				VOC #slot=6				MOVi-D #slot=21, conditional			
	ARI	ARI _{fg}	mIoU	mBO	ARI	ARI _{fg}	mIoU	mBO	ARI	ARI _{fg}	mIoU	mBO	ARI	ARI _{fg}	mIoU	mBO
SLATE-SAM	12.4 _{±1.1}	80.3 _{±0.6}	28.4 _{±0.3}	44.0 _{±0.8}	34.7 _{±0.6}	35.8 _{±1.4}	6.4 _{±0.3}	25.9 _{±0.4}	12.7 _{±0.4}	19.5 _{±0.9}	11.7 _{±0.2}	31.6 _{±1.1}	—	—	—	—
VQSAM _{Tfd}	14.2 _{±1.6}	81.1 _{±0.2}	28.5 _{±0.4}	44.8 _{±0.6}	36.5 _{±0.8}	37.9 _{±0.8}	7.4 _{±0.1}	27.9 _{±0.5}	17.3 _{±0.6}	19.6 _{±0.7}	13.1 _{±0.2}	34.5 _{±0.8}	—	—	—	—
STEVE-SAM	—	—	—	—	—	—	—	—	—	—	—	—	28.0 _{±0.5}	59.3 _{±1.2}	18.0 _{±0.3}	20.3 _{±0.9}
VQSAM _{Tfdt}	—	—	—	—	—	—	—	—	—	—	—	—	39.7 _{±0.2}	68.5 _{±0.8}	24.2 _{±0.2}	26.3 _{±0.4}
DINOSAUR-SAM	14.4 _{±0.3}	87.6 _{±0.9}	25.8 _{±0.7}	39.3 _{±0.7}	27.3 _{±0.4}	27.7 _{±0.5}	5.9 _{±0.1}	22.6 _{±0.5}	11.8 _{±0.7}	16.7 _{±1.1}	11.2 _{±0.3}	29.6 _{±1.2}	—	—	—	—
VQSAM _{MLP}	25.3 _{±2.6}	84.1 _{±0.2}	29.4 _{±1.1}	44.1 _{±0.9}	36.5 _{±0.8}	37.6 _{±0.8}	7.2 _{±0.1}	27.6 _{±0.3}	17.3 _{±0.6}	19.2 _{±0.7}	12.8 _{±0.4}	32.2 _{±0.8}	—	—	—	—
SlotDiffusion-SAM	19.0 _{±1.0}	76.7 _{±2.3}	31.2 _{±0.5}	47.3 _{±1.2}	34.5 _{±0.3}	35.6 _{±0.3}	7.0 _{±0.1}	26.7 _{±0.3}	15.2 _{±0.6}	17.2 _{±1.3}	12.6 _{±0.7}	33.9 _{±1.6}	—	—	—	—
VQSAM _{Dfz}	16.7 _{±0.3}	76.9 _{±0.3}	32.5 _{±0.7}	49.2 _{±0.9}	35.7 _{±0.6}	36.8 _{±0.6}	7.2 _{±0.0}	27.1 _{±0.4}	16.9 _{±1.3}	19.6 _{±1.4}	13.6 _{±0.2}	36.0 _{±0.9}	—	—	—	—

Table 2. Object discovery performance with SAM2 Hiera+FPN (t/16) for OCL decoding. VVO is instantiated as VQSAM; Tfd, Tfdt, MLP and Dfz are Transformer, Transformer-temporal, MLP and Diffusion for OCL decoding respectively.

NOSAUR but is still effective. With a conditional Diffusion model D_{fz} for diffusion decoding, VVO surpasses SlotDiffusion on most datasets.

With supervised pretrained VFMs for OCL encoding, i.e., SAM2 Hierarchical+FPN (version t/16), our VVO is instantiated as VQSAM. As shown in Table 2, VVO consistently boosts those baseline methods’ object discovery performance across all decoding types on most datasets.

As shown in Table 3, whether using a *higher input resolution* or *different aggregators*, VVO maintains its superiority over baselines. As shown in Table 4, VVO outperforms recent *general improvers* for OCL training, i.e., GDR and MSF, which do not support mixture decoding like us though. VVO

	ARI	ARI _{fg}	mIoU	mBO
Using higher resolution: 384×384				
resolution=384×384 COCO (panoptic) #slot=7				
SLATE-DINO	50.9 _{±0.3}	51.0 _{±0.9}	9.0 _{±0.1}	27.9 _{±0.7}
VQDINO _{Tfd}	55.6 _{±0.4}	55.9 _{±0.3}	9.8 _{±0.0}	30.2 _{±0.2}
DINOSAUR-DINO	53.8 _{±0.2}	54.1 _{±0.4}	9.2 _{±0.0}	28.9 _{±0.3}
VQDINO _{MLP}	54.7 _{±0.3}	55.2 _{±0.6}	9.4 _{±0.1}	29.8 _{±0.3}
SlotDiffusion-DINO	53.1 _{±0.6}	53.3 _{±0.8}	9.1 _{±0.2}	28.4 _{±0.7}
VQDINO _{Dfz}	55.3 _{±0.8}	55.7 _{±0.5}	9.8 _{±0.1}	30.2 _{±0.4}
Using different aggregators: SlotAttention, BO-QSA				
resolution=256×256 COCO (panoptic) #slot=7				
SLATE-DINO-SlotAttention	34.1 _{±0.7}	34.9 _{±0.6}	7.0 _{±0.1}	26.2 _{±0.9}
VQDINO _{Tfd} -SlotAttention	37.7 _{±0.5}	39.3 _{±0.4}	7.7 _{±0.1}	28.0 _{±0.6}
SLATE-DINO-BO-QSA	34.4 _{±0.3}	35.4 _{±0.5}	7.1 _{±0.1}	26.8 _{±0.7}
VQDINO _{Tfd} -BO-QSA	38.5 _{±0.4}	39.6 _{±0.4}	7.8 _{±0.0}	28.5 _{±0.4}

Table 3. VVO using higher resolution (*upper*) and different aggregators (*lower*) on object discovery. By default, we use BO-QSA for all our experiment items, including the baselines.

	ARI	ARI _{fg}	mIoU	mBO
Compared with general improvers: GDR and MSF				
resolution=256×256 COCO (panoptic) #slot=7				
GDR _{Tfd} -DINO	34.8 _{±0.4}	36.0 _{±0.6}	7.1 _{±0.1}	27.1 _{±0.7}
MSF _{Tfd} -DINO	35.9 _{±0.3}	37.1 _{±0.4}	7.2 _{±0.0}	27.4 _{±0.5}
VQDINO _{Tfd}	38.5 _{±0.4}	39.6 _{±0.4}	7.8 _{±0.0}	28.5 _{±0.4}
GDR _{Dfz} -DINO	36.2 _{±0.5}	37.1 _{±0.4}	7.1 _{±0.1}	27.2 _{±0.6}
MSF _{Dfz} -DINO	35.6 _{±0.2}	36.6 _{±0.4}	7.1 _{±0.0}	27.2 _{±0.4}
VQDINO _{Dfz}	37.2 _{±0.7}	38.3 _{±0.9}	7.3 _{±0.1}	27.8 _{±0.9}
Compared with SotA methods: SPOT, VideoSAUR				
resolution=256×256 COCO (panoptic) #slot=7				
SPOT-DINO	37.5 _{±0.4}	38.7 _{±0.3}	7.8 _{±0.1}	28.1 _{±0.9}
VQDINO _{Tfd9} +self-training	39.3 _{±0.3}	40.4 _{±0.4}	8.0 _{±0.0}	29.6 _{±0.5}
resolution=256×256 YTVIS (HQ) #slot=7, unconditional				
VideoSAUR-DINO	34.0 _{±0.6}	39.1 _{±0.9}	27.2 _{±0.4}	32.2 _{±0.6}
VQDINO _{Smd}	40.7 _{±0.5}	43.5 _{±0.6}	29.2 _{±0.2}	35.1 _{±0.5}

Table 4. VVO compared with general improvers (*upper*) and SotA methods (*lower*) on object discovery. SPOT uses both Transformer decoder with 9 permutations T_{fd9} and “self-training”; VideoSAUR uses SlotMixer S_{md} as its decoder.

also surpasses *state-of-the-arts*, i.e., SPOT (Kakogeorgiou et al., 2024) and VideoSAUR (Zadaianchuk et al., 2024), with their special types of decoding.

4.3. Evaluate on Set Prediction

	class labels	bounding boxes
	top1 \uparrow	R2 \uparrow
DINOSAUR + MLP	0.61 _{±0.0}	0.57 _{±0.1}
VQDINO _{MLP} + MLP	0.64 _{±0.1}	0.59 _{±0.1}

Table 5. Set prediction performance on COCO (panoptic, #slot=7).

Set prediction task directly shows how much object information those slots grasp. We use OCL to represent dataset COCO as slots, and use a small MLP to predict the object class label and bounding box corresponding to each slot by following this work (Seitzer et al., 2023). We measure top1 accuracy of the classified class labels while we measure the R2 score¹³ of the regressed bounding box coordinates.

As shown in Table 5, compared with baseline DINOSAUR, our VVO, i.e., VQDINO-MLP, obtains better object classification and bounding box regression. Thus, our models’ object representations are of higher quality.

4.4. Deploy to the Downstream

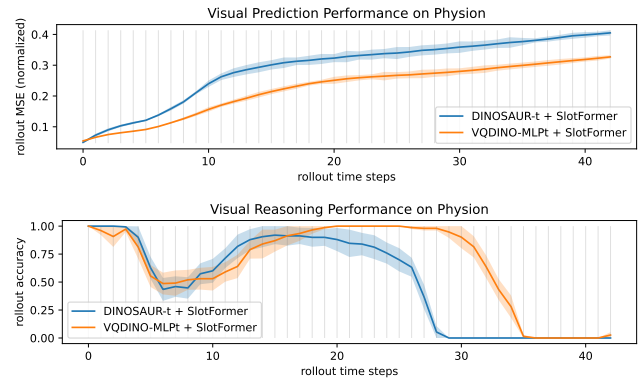


Figure 5. Visual prediction (*upper*) and reasoning (*lower*) performance on Physion (#slot=8). VVO has smaller prediction error in all time steps, and higher reasoning accuracy in later time steps.

Better object representation benefits downstream tasks. We follow the convention to pretrain OCL models on Physion and represent this dataset as slots. Then the object-centric dynamics model SlotFormer (Wu et al., 2023a) is trained on those slots in an auto-regressive manner along the time dimension. We use temporal versions of DINOSAUR and our VVO, i.e., VQDINO-MLP to extract slots.

On *visual prediction*, we evaluate the prediction errors per

¹³https://scikit-learn.org/stable/modules/generated/sklearn.metrics.r2_score.html

	VAE encoding	OCL encoding	VQDINO _{Tfz}	
			ARI	ARI _{fg}
<i>shared</i>	DINO2 ViT	DINO2 ViT	38.5 _{±0.4}	39.6 _{±0.4}
	TAESD encoder	ResNet18	28.3 _{±1.3}	29.1 _{±1.5}
<i>separate</i>	TAESD encoder	DINO2 ViT	34.6 _{±0.7}	35.8 _{±0.5}
	SAM2 encoder	DINO2 ViT	34.9 _{±0.3}	35.8 _{±0.4}

Table 6. VVO’s two key designs: (i) Using VFM representation for encoding is better than using non-VFMs; (ii) Sharing the OCL encoder as VAE encoder to obtain targets is better than using separate VAE and OCL encoders. Results are on COCO panoptic.

shared VAE / OCL encoder	Gumbel noise	annealing residual	normaliz. regulariz.	VQDINO _{Dfz}	
				ARI	ARI _{fg}
✓	✓	✓	✓	37.2 _{±0.7}	38.3 _{±0.9}
✗	✓	✓	✓	35.4 _{±2.5}	36.6 _{±2.2}
✓	✓			36.5 _{±1.6}	37.6 _{±1.9}
✓		✓		36.8 _{±1.3}	37.8 _{±1.0}
✓			✓	36.9 _{±0.7}	37.9 _{±0.8}

Table 7. VVO’s VQ variant: All our three tricks are beneficial to the overall performance boosts. In comparison to VVO’s key designs, these tricks are more like the cherry on top. Results are on COCO panoptic with settings consistent with the above.

time step measured in normalized MSE between regressed and extracted slots. As shown in Figure 5 upper, VVO accumulates prediction errors slower than the baseline.

On *visual reasoning*, we evaluate the reasoning accuracies per time step between classified and ground-truth labels. As shown in Figure 5 lower, VVO accuracies are slightly lower at the beginning but much higher later than the baseline.

4.5. Ablate the Architecture

As shown in Table 6, VVO’s design of *shared VAE and OCL encoder* consistently outperforms separate VAE and OCL encoders, even when the latter employs another VFM for VAE encoding. Thus, VVO’s design of shared VFM representation quantization is crucial. However, the design of separate encoders remains prevalent among those baselines.

As shown in Table 7, VVO’s *improved quantizer variant*, based on tricks of Gumbel noises defined in Equation (13), annealing residual connection defined in Equation (14) and normalizing regularization defined in Equation (15), is superior to the naive VQ. The detailed effects of those tricks are shown in Figure 6. *Adding Gumbel noises* increases codebook utilization, contributing to more effective codes; *Annealing residual connection* improves VAE pretraining, contributing to smaller VAE reconstruction error.

Conclusion

We propose a unified architecture VVO for object-centric representation learning. Our VVO supports different well-recognized vision foundation models for OCL encoding and

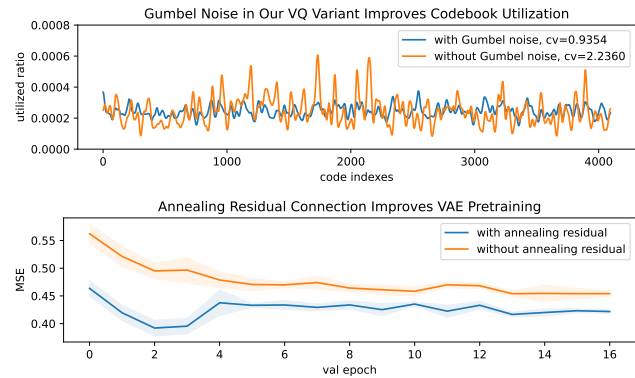


Figure 6. Effects of tricks in our VQ variant: (upper) Gumbel noise improves codebook utilization, where “CV” means Coefficient of Variation, and curves are smoothed by Gaussian kernel of size 10; (lower) Annealing residual connection improves VAE pretraining, and the blue curve’s turning point at epoch 4 is where the residual connection anneals to zero. Results are from the VAE pretraining of VQDINO-_{Dfz} on COCO panoptic.

supports mainstream types of OCL decoding. It boosts the existing OCL performance in object discovery significantly, and benefits downstream tasks of visual prediction and reasoning. VVO has the potential to serve as a general testbed for research related to OCL in the future.

Impact Statement

This paper presents work whose goal is to advance the field of Machine Learning. There are many potential societal consequences of our work, none which we feel must be specifically highlighted here.

References

- Bar, M. Visual Objects in Context. *Nature Reviews Neuroscience*, 5(8):617–629, 2004.
- Bengio, Y., Leonard, N., and Courville, A. Estimating or Propagating Gradients through Stochastic Neurons for Conditional Computation. *arXiv preprint arXiv:1308.3432*, 2013.
- Biza, O., van Steenkiste, S., Sajjadi, M. S., Elsayed, G., Mahendran, A., and Kipf, T. Invariant Slot Attention: Object Discovery with Slot-Centric Reference Frames. In *International Conference on Machine Learning*, pp. 2507–2527, 2023.
- Caron, M., Touvron, H., Misra, I., et al. Emerging Properties in Self-Supervised Vision Transformers. In *Proceedings of the IEEE/CVF International Conference on Computer Vision*, pp. 9650–9660, 2021.

- Cavanagh, P. Visual Cognition. *Vision Research*, 51(13): 1538–1551, 2011.
- Elsayed, G., Mahendran, A., Van Steenkiste, S., et al. SAVi++: Towards End-to-End Object-Centric Learning from Real-World Videos. *Advances in Neural Information Processing Systems*, 35:28940–28954, 2022.
- Ge, S., Mishra, S., Kornblith, S., Li, C.-L., and Jacobs, D. Hyperbolic Contrastive Learning for Visual Representations Beyond Objects. In *Proceedings of the IEEE/CVF conference on computer vision and pattern recognition*, pp. 6840–6849, 2023.
- Greff, K., Kaufman, R. L., Kabra, R., et al. Multi-Object Representation Learning with Iterative Variational Inference. In *International Conference on Machine Learning*, pp. 2424–2433. PMLR, 2019.
- He, K., Zhang, X., Ren, S., and Sun, J. Deep Residual Learning for Image Recognition. In *Proceedings of the IEEE conference on computer vision and pattern recognition*, pp. 770–778, 2016.
- Im Im, D., Ahn, S., Memisevic, R., and Bengio, Y. Denoising criterion for variational auto-encoding framework. In *Proceedings of the AAAI conference on artificial intelligence*, volume 31, 2017.
- Jia, B., Liu, Y., and Huang, S. Improving Object-centric Learning with Query Optimization. In *The Eleventh International Conference on Learning Representations*, 2023.
- Jiang, J., Deng, F., Singh, G., and Ahn, S. Object-Centric Slot Diffusion. *Advances in Neural Information Processing Systems*, 2023.
- Kakogeorgiou, I., Gidaris, S., Karantzas, K., and Komodakis, N. SPOT: Self-Training with Patch-Order Permutation for Object-Centric Learning with Autoregressive Transformers. In *Proceedings of the IEEE/CVF Conference on Computer Vision and Pattern Recognition*, pp. 22776–22786, 2024.
- Kipf, T., Elsayed, G., Mahendran, A., et al. Conditional Object-Centric Learning from Video. *International Conference on Learning Representations*, 2022.
- Kirillov, A., Mintun, E., Ravi, N., Mao, H., Rolland, C., Gustafson, L., Xiao, T., Whitehead, S., Berg, A. C., Lo, W.-Y., Dollar, P., and Girshick, R. Segment Anything. In *Proceedings of the IEEE/CVF International Conference on Computer Vision (ICCV)*, pp. 4015–4026, October 2023.
- Krizhevsky, A., Sutskever, I., and Hinton, G. ImageNet Classification with Deep Convolutional Neural Networks. *Advances in Neural Information Processing Systems*, 25, 2012.
- Locatello, F., Weissenborn, D., Unterthiner, T., et al. Object-Centric Learning with Slot Attention. *Advances in Neural Information Processing Systems*, 33:11525–11538, 2020.
- Oquab, M., Darcet, T., Moutakanni, T., et al. DINOv2: Learning Robust Visual Features without Supervision. *Transactions on Machine Learning Research*, 2023.
- Palmeri, T. and Gauthier, I. Visual Object Understanding. *Nature Reviews Neuroscience*, 5(4):291–303, 2004.
- Ravi, N., Gabeur, V., Hu, Y.-T., Hu, R., Ryali, C., Ma, T., Khedr, H., Rädle, R., Rolland, C., Gustafson, L., et al. SAM 2: Segment Anything in Images and Videos. *arXiv preprint arXiv:2408.00714*, 2024.
- Seitzer, M., Horn, M., Zadaianchuk, A., et al. Bridging the Gap to Real-World Object-Centric Learning. *International Conference on Learning Representations*, 2023.
- Singh, G., Deng, F., and Ahn, S. Illiterate DALL-E Learns to Compose. *International Conference on Learning Representations*, 2022a.
- Singh, G., Kim, Y., and Ahn, S. Neural Systematic Binder. *International Conference on Learning Representations*, 2022b.
- Singh, G., Wu, Y.-F., and Ahn, S. Simple Unsupervised Object-Centric Learning for Complex and Naturalistic Videos. *Advances in Neural Information Processing Systems*, 35:18181–18196, 2022c.
- Uijlings, J. R., Van De Sande, K. E., Gevers, T., and Smeulders, A. W. Selective Search for Object Recognition. *International Journal of Computer Vision*, 104:154–171, 2013.
- Van Den Oord, A., Vinyals, O., and Kavukcuoglu, K. Neural Discrete Representation Learning. *Advances in Neural Information Processing Systems*, 30, 2017.
- Vaswani, A., Shazeer, N., Parmar, N., et al. Attention Is All You Need. *Advances in Neural Information Processing Systems*, 30, 2017.
- Wang, X., Misra, I., Zeng, Z., Girdhar, R., and Darrell, T. VideoCutler: Surprisingly Simple Unsupervised Video Instance Segmentation. In *Proceedings of the IEEE/CVF Conference on Computer Vision and Pattern Recognition*, pp. 22755–22764, 2024.
- Watters, N., Matthey, L., Burgess, C. P., and Lerchner, A. Spatial Broadcast Decoder: A Simple Architecture for Learning Disentangled Representations in VAEs. *arXiv preprint arXiv:1901.07017*, 2019.

- Wu, Z., Dvornik, N., Greff, K., Kipf, T., and Garg, A. SlotFormer: Unsupervised Visual Dynamics Simulation with Object-Centric Models. *International Conference on Learning Representations*, 2023a.
- Wu, Z., Hu, J., Lu, W., Gilitschenski, I., and Garg, A. SlotDiffusion: Object-Centric Generative Modeling with Diffusion Models. *Advances in Neural Information Processing Systems*, 36:50932–50958, 2023b.
- Yang, D., Liu, S., Huang, R., et al. Hifi-Codec: Group-Residual Vector Quantization for High Fidelity Audio Codec. *arXiv preprint arXiv:2305.02765*, 2023.
- Zadaianchuk, A., Seitzer, M., and Martius, G. Object-Centric Learning for Real-World Videos by Predicting Temporal Feature Similarities. *Advances in Neural Information Processing Systems*, 36, 2024.
- Zhao, R., Wang, V., Kannala, J., and Pajarinen, J. Grouped Discrete Representation for Object-Centric Learning. *arXiv preprint arXiv:2411.02299*, 2024a.
- Zhao, R., Wang, V., Kannala, J., and Pajarinen, J. Multi-scale fusion for object representation. *arXiv preprint arXiv:2410.01539*, 2024b.
- Zhu, Y., Li, B., Xin, Y., and Xu, L. Addressing Representation Collapse in Vector Quantized Models with One Linear Layer. *arXiv preprint arXiv:2411.02038*, 2024.

A. Dataset Processing

The datasets for image OCL are ClevrTex, COCO (panoptic) and VOC. The datasets for video OCL are MOVi-D and YTVIS. For different datasets, we have mostly the same processing but a bit differences.

A.1. Shared Preprocessing

To accelerate experiments, we adopt the dataset conversion scheme: Convert all datasets into LMDB database format, and load it into NVMe disk or RAM disk to minimize I/O overhead and maximize throughput.

Specifically, all images or video frames are resized by short side to 256, as well as their segmentation masks, and then are stored data type uint8 to save space. For images or videos, we use default interpolation mode; but for segmentation masks, we use NEAREST-EXACT interpolation mode.

During training, for both images and videos, we use spatial resolution of 256×256 as inputs and outputs. We normalize the input images or videos by ImageNet-Mean and -Std, which are the common normalization scheme using by VFMs like DINO and SAM. For videos, we also using random strided temporal cropping of fixed window size 6 to accelerate training and improve generalization.

During testing, there is no difference to that of training for images. But for videos, we need to remove the random strided temporal cropping and use the full video of 24 time steps.

A.2. Dataset-Specific Processing

ClevrTex. As there are 10 objects at most in each image, we use number of slots queries of $10 + 1$, where 1 represents for the background.

COCO & VOC. We use the panoptic segmentation annotations of COCO for evaluation, which is more challenging than instance segmentation. Besides, OCL’s queries-based workflow intuitively fits panoptic segmentation rather than instance segmentation or semantic segmentation. There can be lots of or only two objects in an image, but we just follow the popular hyperparameter selection, i.e., 7 slots for COCO and 6 slots for VOC, respectively.

MOVi-D. There are abundant annotations like depth, optical-flow, camera intrinsic/extrinsic parameters and so on. But for simple comparison, we only utilize the segmentation masks for evaluation and the bounding boxes as slots initialization. As there are 23 objects in these dataset, we use number of slots queries of $23+1$.

YTVIS. We use the original YTVIS videos and HQ-YTVIS segmentation annotations. The latter provides high-quality masks. During VAE pretraining, we utilize all the video frames. But during OCL training, we only utilize the every-5-time-step annotations for calculating the performance.

B. Training Recipe

Following the convention, there are two training stages. The pretraining stage is for training VAE modules on corresponding datasets, so as to learn good discrete intermediate representation. The OCL training stage, which utilize the pretraining VAE representation as guidance for object centric learning.

B.1. Pretrain VAE

For all datasets, we use total number of training iterations 30,000, and validation interval iterations 600, so that we have about 50 checkpoints for every OCL model on every dataset. But to save storage, we save only the latter half 25 checkpoints. This is unified across all datasets.

The batch size for image datasets is 64, while for video datasets it is 16. This holds for both training and validation. This setting is shared across all datasets.

For multi-process, we use the number of workers 4. This holds for both training and validation. This setting is shared across all datasets.

We use Adam optimizer with initial learning rate of $2e-3$. And the learning rate is manipulated by cosine annealing scheduling, with a linear warmup during first $1/20$ of total steps. This setting is shared across all datasets.

We use automatic mixed precision provided by PyTorch autocast API plus compile. Along with this, we use PyTorch builtin gradient scaler, so as to apply gradient clipping of maximum norm 1.0. This setting is shared across all datasets.

B.2. Train OCL Model

For all datasets, we use total number of training iterations 5,0000, and validation interval iterations 1000, so that we have about 50 checkpoints for every OCL model on every dataset. But to save storage, we only save the latter half of the total checkpoints. This setting is shared across all datasets.

The batch size for image datasets is 32 for both training and validation, while for video datasets it is 8 for training and 4 for validation as there are more time steps in videos during validation. This setting is shared across all datasets.

For multi-process, we use the number of workers 4. This holds for both training and validation. This setting is shared across all datasets.

The objective is the CE and MSE loss following the basis methods original design.

Metrics used here are ARI, mIoU and mBO, calculating the panoptic segmentation accuracy of both objects and the background. This setting is shared across all datasets.

We use Adam optimizer with initial learning rate of $2e-4$. And the learning rate is manipulated by cosine annealing scheduling, with a linear warmup during first 1/20 of total steps. This setting is shared across all datasets.

We use auto mixed precision provided by PyTorch autocast API and compile. Along with this, we use PyTorch builtin gradient scaler, so as to apply gradient clipping of maximum norm 1.0 for images and 0.02 for videos.